Quality Assessment of Metal Traces Manufactured by Localized Electrochemical Deposition Printing and Electroless Plating

Moein Khakzad[1], Amirhossein Shafieizad[2], Maria Josefina Arellano-Jimenez[3], Mohammadreza Mahmoudi[4], Jagannathan Rajagopalan[4], Majid Minary-Jolandan[1*]

[1]Department of Mechanical Engineering, The University of Texas at Dallas, Richardson, Texas 75080, United States.
[2]Materials Science and Engineering, School for Engineering of Matter, Transport and Energy, Arizona State University, Tempe, AZ 85287, United States.
[3]Department of Materials Science and Engineering, The University of Texas at Dallas, Richardson, TX 75080, USA.
[4]Mechanical and Aerospace Engineering, School for Engineering of Matter, Transport and Energy, Arizona State University, Tempe, AZ 85287, United States.

*Corresponding author E-mail: majid.minary@utdallas.edu

ABSTRACT: In the quest for more compact and efficient electronic devices, the manufacturing of circuit traces has undergone significant innovations. Traditional subtractive methods like photolithography, while effective, are costly and require cleanroom facilities. Additive manufacturing, particularly 3D printing technologies, offers cost-effective alternatives. Among these, Confined Electrodeposition (CED) stands out for its precise control over metal microstructure, enabling the printing of high-conductivity metals such as copper and nickel. This study focuses on assessing the quality of circuit traces produced using a hybrid approach that combines localized electrodeposition printing and electroless plating. Utilizing microscopy and high throughput nanoindentation (~10,000 indentations) techniques, we observed both uniform and non-uniform regions within the metal traces, attributing the inconsistencies primarily to the electroless plating step. Our findings contribute insights for the future design and fabrication of circuit traces in printed electronics, circuit boards, and electronic packaging.

KEYWORDS: Metallic Traces, Printed Electronics, Electroless Plating, Localized Electrodeposition Printing, Quality Assessment.

1. Introduction

In recent years, the demand for more compact, efficient, and multifunctional electronic devices has been on the rise [1]. This trend has necessitated advancements in the manufacturing technologies of various components, including circuit traces, which are essential in electronic packaging and circuit boards [2-6]. Traditionally, circuit traces have been fabricated using subtractive manufacturing methods like photolithography, which can be costly, time-consuming, and less environmentally friendly due to waste generation. Considering these challenges, additive manufacturing technologies, commonly referred to as 3D printing, have emerged as an appealing alternative to produce circuit traces [7]. Processes like direct ink writing (DIW) [8], electrohydrodynamic printing (EHD) and inkjet printing [9], liquid metal printing [10, 11] , laser-induced forward transfer (LIFT) and electrochemical printing [12, 13] offer a degree of flexibility and cost-effectiveness that is not readily achievable through conventional means.

Among these methods, confined electrodeposition (CED) has demonstrated exceptional control over the microstructure of printed metal [14-17], facilitating the direct printing of high-conductivity (< 2-times of the bulk conductivity) metals such as copper (Cu) and nickel (Ni) onto various substrates [18-23]. It is also possible to print alloys using this technique by co-electrodeposition from a single electrolyte [24]. Electroless plating can be combined with electroplating or direct ink writing for development of hybrid printing technologies [25, 26]. Both electroplating and electroless plating are low-cost and scalable techniques for such applications and hence are appealing from engineering point of view [2, 26-30].

In this work, we analyze the quality of multi-layer metal traces fabricated by combined CED and electroless plating, in which electroless Cu layer was deposited on 3D printed Ni patterns generated by electroplating. Our microscopy results revealed non-uniform regions in the fabricated

traces, primarily due to inconsistencies in the electroless plating step. In addition, we characterize the mechanical properties of the fabricated metal traces using a high throughput nanoindentation technique (~10,000 indentations) to create continuous maps. The results of this work will be useful for design and fabrication of circuit traces in printed electronics, circuit boards, and electronic packaging.

2. Results and discussion

The fabrication process begins with the deposition of a blanket Cu film on a Ti-coated Si wafer (Steps 1 and 2, Figure 1). The Cu-coated substrate is then placed in a custom-built electrochemical 3D printer, where desired interconnect patterns are printed through the CED process (Step 3). At this stage, a pattern of Ni film is printed on the substrate [18]. CED operates on the principle of localized electrochemical deposition. The process employs an aqueous electrolyte-filled nozzle to deposit thin films of metal or alloy on a conductive substrate, all controlled by a 3D positioning system. In this method, an electrolyte-filled nozzle, typically equipped with a metal electrode, is moved along predetermined paths above a substrate. An electric potential is applied between the nozzle electrode and the substrate, promoting the reduction of metal cations in the electrolyte to their metallic state. This results in the localized deposition of metal directly underneath the nozzle. Following the printing of the interconnect pattern, the blanket film is removed by wet etching (Step 4).

This printed pattern serves as a seed layer for the subsequent electroless deposition process (Step 5). We utilized commercial Cu electroless plating solutions. In electroless plating, metal ions in a chemical solution are reduced onto the surface of the material, forming a metal coating. Unlike electroplating, which requires electrical input, electroless plating is solely reliant on a chemical

reaction to induce metal deposition [27]. In our process, the printed Cu confines Cu plating to the Ni traces printed on the substrate.

The bottom right of Figure 1 shows chemical composition maps that are overlaid on a high-angle annular bright field (HAABF) cross-section image recorded in STEM mode for enhanced presentation. The nozzle speed in the CED process controls the thickness of the printed Ni [18], while the thickness of the electroless deposited Cu is mainly controlled by deposition time (here, 80 - 85 nm/min). The width of the fabricated trace is also controlled by nozzle speed as well as the nozzle diameter since electroplating is confined to the nozzle tip [20].

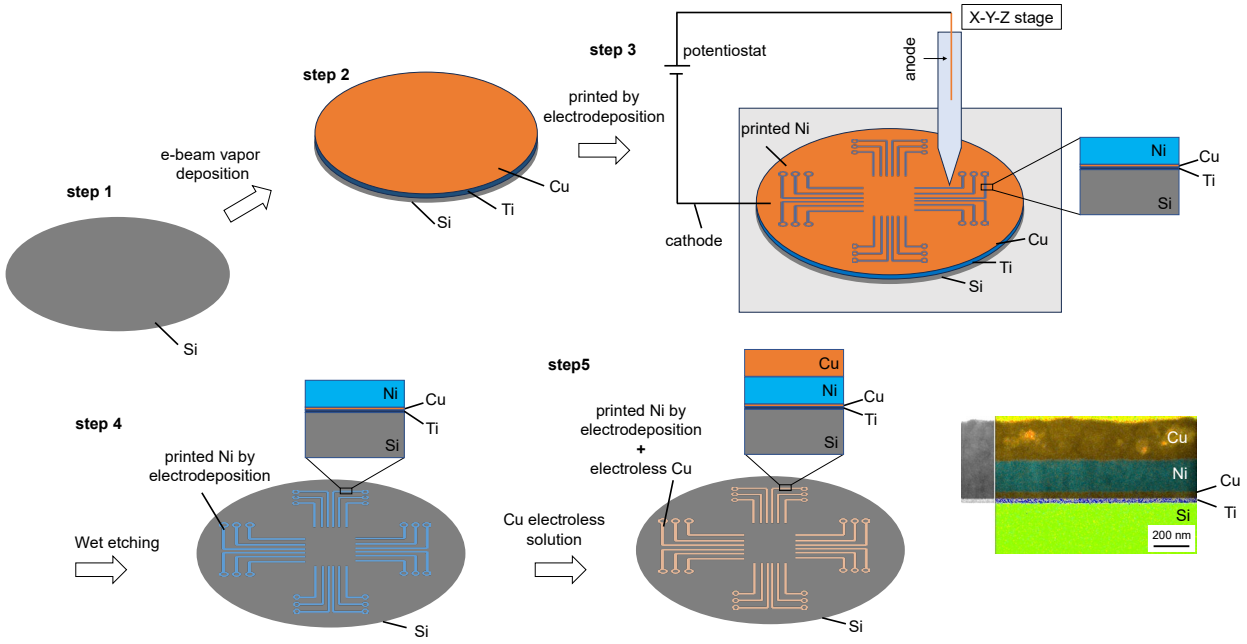

Figure 1 Schematic of the fabrication process for copper interconnects. The process involves the deposition of a blanket Cu film on a Ti-coated Si wafer, followed by 3D printing of Ni using the confined electrodeposition (CED) process. Subsequently, the blanket Cu film is etched, and Cu is electroless plated in controlled areas. The bottom right shows chemical composition maps overlaid on a high-angle annular bright field (HAABF) cross-section image recorded in STEM mode for enhanced presentation.

After printing, we used optical microscopy to examine the fabricated traces. We observed two general characteristics: regions with uniform films (Figure 2A) and regions with non-uniform films (Figure 2D). The uniform regions appeared bright in optical images, while the non-uniform regions appeared darker. In top-view SEM images, the uniform region exhibited nearly full coverage of the substrate, albeit with some small holes (Figure 2B). In the non-uniform regions, we noticed globular-like growths and patches where no film had grown (Figure 2E).

To investigate this observed non-uniformity, we conducted cross-sectional STEM imaging (Fig 2C and F). Figures S1-S3 show process steps for sample preparation to obtain STEM images. In a STEM image from a uniform region, we could clearly identify the electroplated Ni layer, with a thickness of approximately 180 nm. Above this Ni layer, we observed a uniform electroless plated Cu layer, with an average thickness of 220 nm. The cross-sectional STEM image from a non-uniform region clearly showed that the electroplated Ni layer was uniform (Figure 2F). The observed non-uniformity originated from the electroless plating step. Figure 2F revealed that the electroless plated Cu layer was non-uniform, with variations in thickness ranging from approximately ~130 nm to ~400 nm. Additional top-view and cross-sectional SEM images of both uniform and non-uniform regions are presented in Figures 3-4.

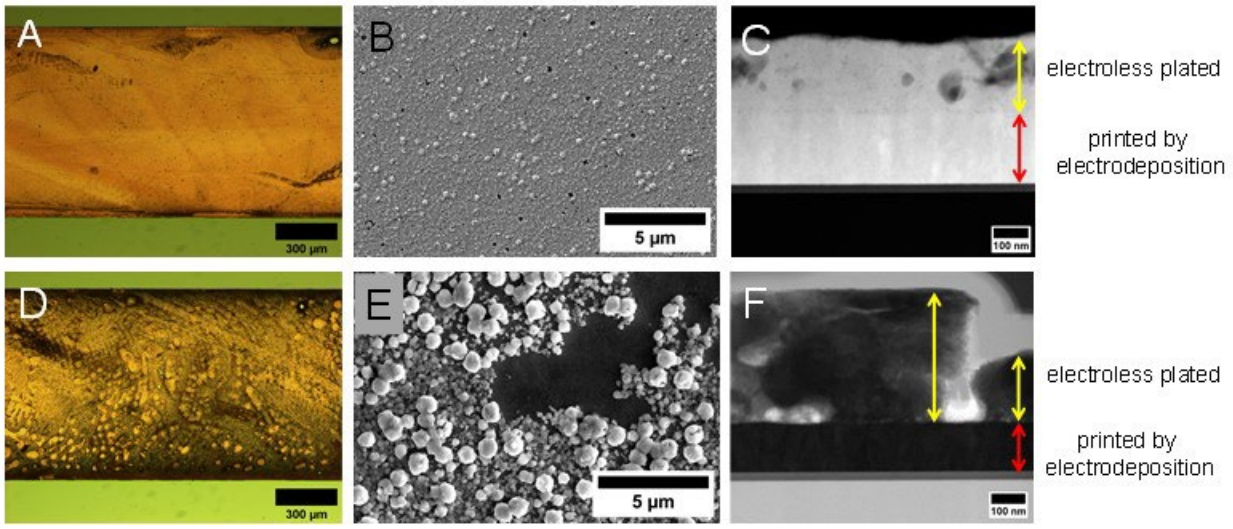

Figure 2 (A)-(C) Top-view optical and SEM images, as well as a cross-sectional dark-field STEM image, obtained from a uniform region on the Si wafer, respectively. (D)-(F) Top-view optical and SEM images, along with a cross-sectional bright-field STEM image, obtained from a non-uniform region on the Si wafer, respectively. In the cross-sectional images in panels C and F, the films printed by electroplating and plated by electroless deposition are indicated with arrows.

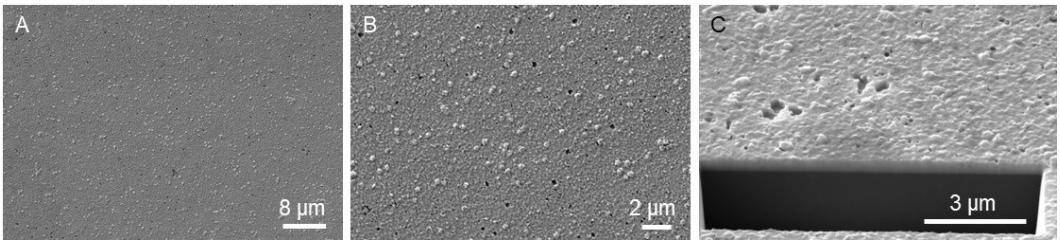

Figure 3 SEM images of the film at uniform regions.

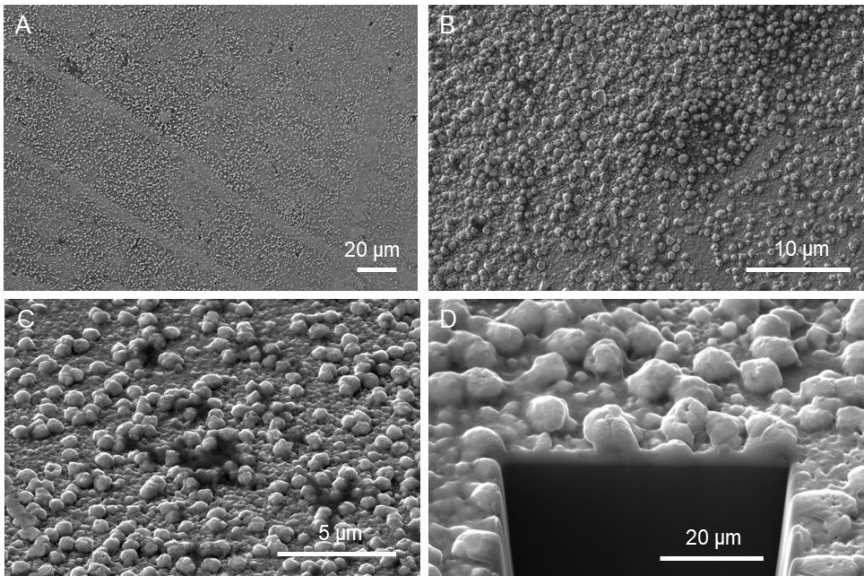

Figure 4 SEM images of the film at non-uniform regions.

A cross-sectional sample from a non-uniform region was prepared to verify the existence, extent, and efficiency of the electroless-plated layer in areas where irregular growth was observed,

and to compare it with data obtained from uniform regions (Figure 5). Figure 5A shows the STEM bright-field (BF) image of the typical multilayer arrangement present in the uniform region. As described in the fabrication process, the successive layers of Ti and Cu on top of Si are evident in the elemental maps in Figure 5A. The presence of oxygen below the metals aligns with a native SiO_2 layer, followed by the electrodeposited Ni layer and electroless-plated Cu layers.

Regarding the sample from the non-uniform region, the cross-sectional image and maps are shown in Figure 5B. The Cu, Ti, Si, and O on the Si wafer are consistent with the homogeneous region, as observed in the corresponding elemental maps. The electrodeposited Ni layer is also homogeneous. The Cu maps reveal an irregular Cu coating: some areas are completely covered, some have a thin coating, and some areas are uncoated. Additionally, the Si and O maps in Figure 5 indicate the presence of a SiO_2 layer that was deposited on top of the samples during FIB preparation, observed in the top section of both samples (Figure S1-S3).

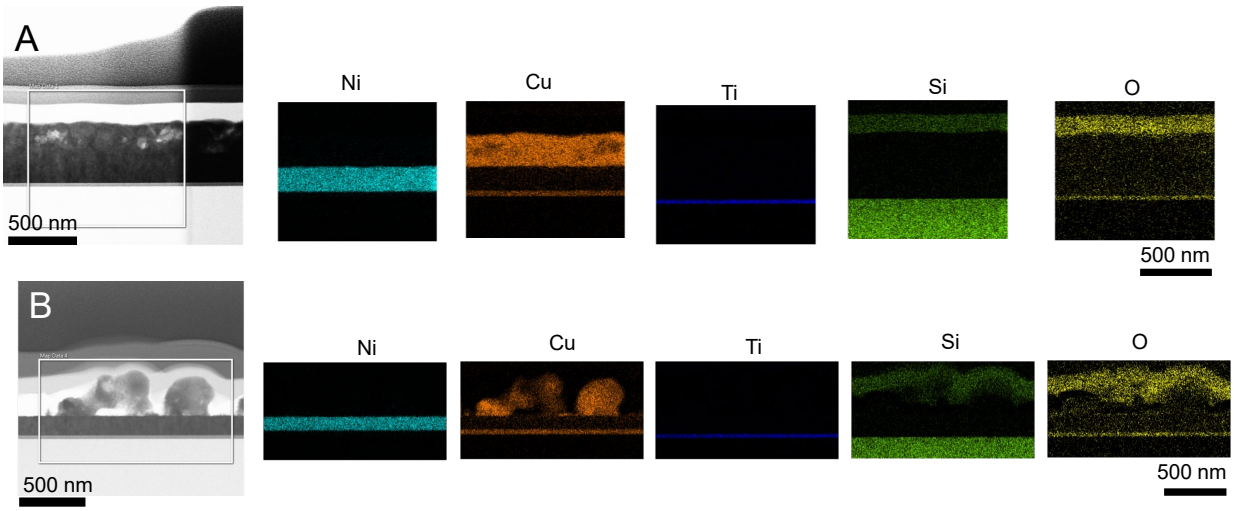

Figure 5 High-angle annular bright field images obtained in STEM mode from (A) a uniform region and (B) non-uniform region on the Si wafer. (Note that the scale bars are different.)

The electroless process is autocatalytic, meaning that the metal being deposited acts as a catalyst to promote its own deposition [27, 29]. Mechanistically, electroless copper deposition proceeds in two steps: the thin-film stage (up to 3 μm) and the bulk stage (often 1-15 μm). In this work, the electroless deposited Cu was less than 500 nm and thus well within the thin-film range. Electroless Cu thin films, with a thickness up to 1 μm, typically consist of small (0.2 μm) equiaxial grains. The formation of the thin film involves three concurrent processes contributing to crystal structure development: nucleation, or the initiation of new crystals; growth, or the enlargement of these crystals; and coalescence, or the merging of three-dimensional crystallites (TDCs) [27].

In the initial phase of electroless copper deposition, the average number of TDCs grows as the deposition time increases, with nucleation being the dominant activity. Subsequently, the average TDC density peaks and then starts to decline. During this period of declining TDC density, coalescence becomes the primary mechanism for building the crystal structure. A seamless electroless film is created through the side-by-side expansion and merging of TDCs. The physical qualities of the deposit are influenced by the kind of coalescence. Two forms of TDC coalescence exist: the first, where coalescence occurs without fully occupying the space between TDCs, can lead to impurities, stress, voids, and dislocations; and the second, where the space between TDCs is filled, results in higher-quality copper compared to the first type. The manner of coalescence is largely influenced by the type and concentration of additives in the solution. Additionally, the quality of the underlying substrate may affect nucleation and coalescence behavior. In our process, it is likely that improvements in the quality of the printed Ni layer should be investigated in future studies to determine to what extent the quality of the Ni layer affects the nucleation and coalescence of the TDCs. It is likely that pinholes, topographic roughness, and local metal composition may affect these processes.

We used nanoindentation with a Berkovich tip to measure the indentation modulus and hardness of the films in the uniform region. To assess the nanomechanical properties of the sample over a wide range of areas, we employed the NanoBlitz3D technique [31]. This high-speed indentation testing technique enables rapid mapping of material properties, unlike traditional indentation methods. NanoBlitz3D applied a specified load to the sample and measured the resulting indentation depth and contact stiffness. These values were then converted into hardness and elastic modulus using the Oliver-Pharr indentation model [32]. To achieve this, we conducted an indentation experiment that covered a substantial portion of the surface area under investigation, performing roughly 10,000 individual indents in total on the specimen with a load of 1.2 mN. To prevent the formation of plastic-affected zones near each indentation, the distance between each indent was set to 10 μm.

The NanoBlitz3D nanoindentation technique was applied onto fabricated Cu pattern by indenting an array of 20×160 (3200 points) in an area of 1600×200 μm^2 shown in Figure 6A. The mean values of the indentation modulus (E) and hardness (H) were measured to be 121 ± 19 GPa and 2.78 ± 0.73 GPa, respectively. A rather uniform distribution of light green, as seen in Figure 6B and C, is close to the mean value in 2D contours and verifies a homogeneous distribution of mechanical properties. Distributions of indentation elastic modulus and hardness are shown in Figures 6D and 6E. The dashed lines represent the corresponding normal distribution plots.

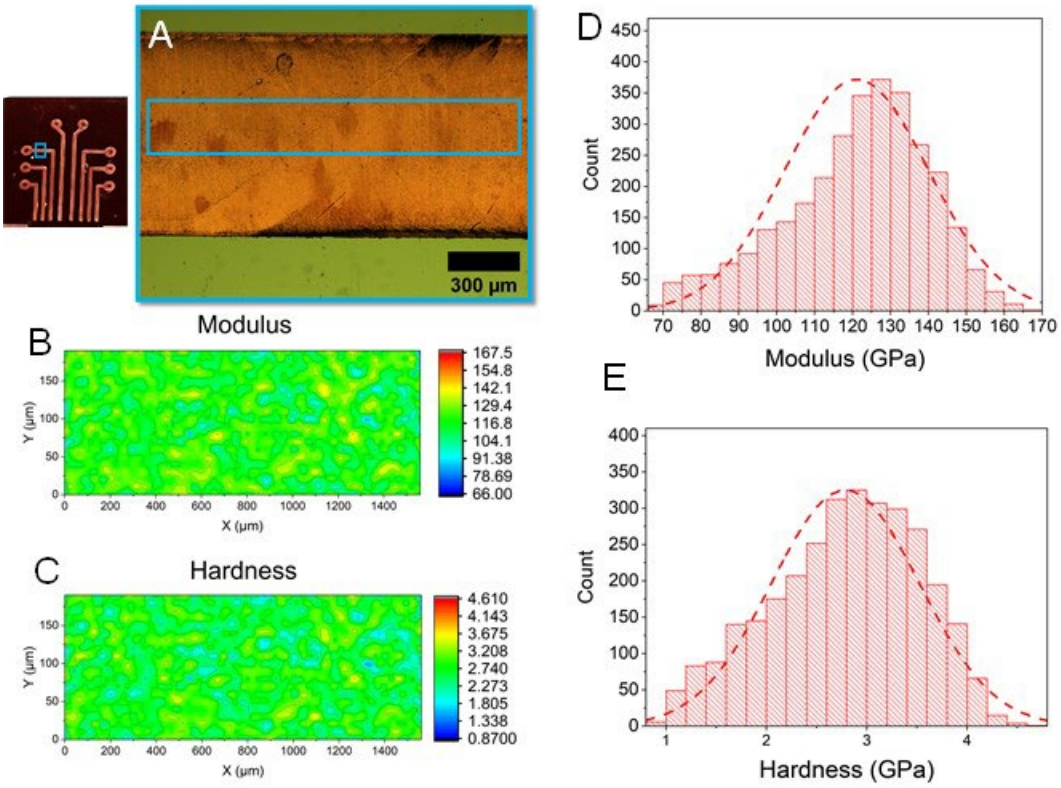

Figure 6 (A) The area of 1600×200 µm^2, on which 3,200 indents were applied using the NanoBlitz3D technique. (B) and (C) are nanoindentation modulus and hardness 2D contour plots obtained. (D) and (E) show the distribution of modulus and hardness values for the selected area, respectively.

To compare our results with reference material, the same test was conducted on bulk copper. An array of NanoBlitz3D footprints, each with 400 indents, is shown in Figure 7A. The mean value of the modulus was 133.2 ± 4.24 GPa. When comparing the normal distribution plots in Figures 7B and 7C, it becomes evident that the fabricated metal traces in this work show a broader distribution than the bulk copper; however, statistically, both materials have the same elastic modulus. The large variation in data for the fabricated traces could be attributed to defects generated during manufacturing (Figure S4). Additionally, the multi-layer nature of the interconnect may also affect the obtained elastic modulus.

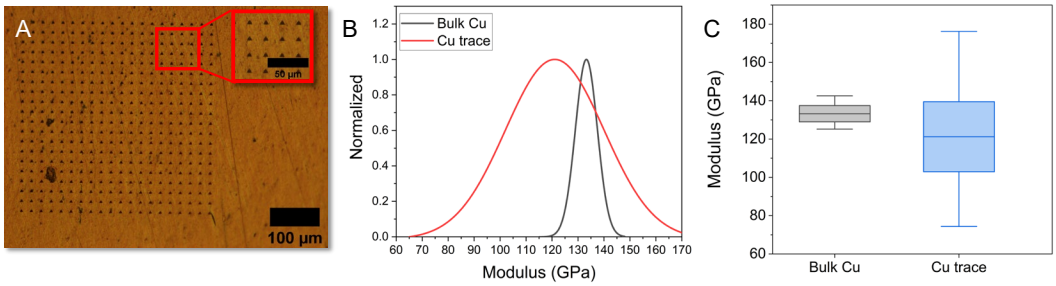

Figure 7 (A) An optical image of an array of nanoindentation footprints on bulk Cu. (B) and (C) Comparison of the elastic modulus between bulk Cu and fabricated interconnected Cu.

EXPERIMENTAL SECTION

Materials: For electroplating printing, the Ni electrolyte used was the classical Watts's bath. This bath consisted of 0.5M $NiSO_4 \cdot 6H_2O$ (Sigma-Aldrich), 0.1M $NiCl_2$ (Sigma-Aldrich), and 0.7M H_3BO_3 (Sigma-Aldrich) in deionized (DI) water. A Ni wire, approximately 0.3 mm in diameter, was inserted from the backside of the plastic syringe to serve as the anode. The substrate for printing, which acted as the cathode, was a silicon wafer. To remove the Cu blanket layer, a Cu etchant (APS-100, Transene Company, Inc.) was used, which consists of 15-20% ammonium peroxydisulfate and 80-85% water by weight. For electroless plating, electroless Cu solutions A and B from Transene Company, Inc. were utilized.

Fabrication of the Metallic Pattern: A silicon wafer was initially coated with thin layers of titanium (Ti) and copper (Cu) using e-beam evaporation. For nickel (Ni) printing via electroplating, a plastic syringe served as the printing head. This syringe was connected to a syringe pump to regulate the flow of the electrolyte through the nozzle. A constant voltage of -1.2 V was maintained during the Ni printing process. Wet etching was then carried out to remove the unprinted initial Cu layer. After the removal of this initial conductive metallic layer, the printed

substrate was immersed in Cu electroless plating solutions following the manufacturer guidelines. The nominal deposition rate is ~ 84 nm/min. Following removal from the plating solution, the samples were rinsed with deionized (DI) water.

Nanoindentation: The mapping of material properties was rapidly conducted using a NanoFlip nanoindenter, which was equipped with a Berkovich tip and utilized the high-speed indentation testing technique known as NanoBlitz3D. The NanoBlitz3D methodology involves applying a specified load to the sample, followed by measuring the resulting indentation depth and contact stiffness. These measured values are then converted into hardness and elastic modulus values through the Oliver-Pharr indentation model. The NanoBlitz nanoindentation technique was applied over a vast area of the Cu pattern, creating approximately 10,000 indents. The indents were arranged in arrays ranging from 20×20 (comprising 400 points within an area of 1600×200 μm^2) to 20×160 (comprising 3200 points within an area of 1600×200 μm^2), with an applied load of 1.2 mN. To avoid the formation of plastic-affected zones near each indentation, the distance between each indent was set at 10 µm. Additionally, to mitigate errors due to thermal drift during measurement, a thermal drift rate of approximately 0.2 nm/s was established before initiating the tests.

Microscopy: For cross-section observation and elemental analysis, a standard TEM-lamella preparation was done using a Focused Ion Beam (FIB) System Nova200 Nanolab (FEI-TermoFisher). The dual beam system operated using an acceleration voltage from 30 kV to 5 kV for progressive milling and the gas injection system that includes Pt, SiO_2, and C for protective-layer deposition. TEM and STEM imaging performed using a Cs-corrected JEOL Scanning-Transmission Electron Microscope JEM-ARM200F, operated at 200 kV. Bright-field (BF) and

high-angle annular dark field (HAADF) detectors used for imaging. Chemical analysis (maps) acquired using Energy Dispersive Spectroscopy (EDS) Aztec X-MaxN, Oxford Instruments.

Conclusions

In conclusion, this study presents a hybrid technique employing confined electrodeposition 3D printing and electroless plating for the fabrication of copper traces, a critical component in modern electronic and energy systems. Microscopy results indicate both uniform and non-uniform regions in the fabricated interconnects, with inconsistencies in the electroless plating step identified as a primary factor. We explore a potential mechanism for this and investigate the mechanical properties through high throughput nanoindentation techniques. While the elastic modulus of the fabricated interconnects closely aligns with that of bulk copper, a broader distribution of mechanical properties exists, potentially due to manufacturing defects or the multi-layered nature of the interconnects. Future research should aim to identify the exact mechanisms contributing to non-uniform coatings and to develop new strategies for the fabrication of large-scale, uniform metallic traces using this hybrid approach.

Supporting information: Figures S1-S4: Sample preparation steps for STEM imaging. Dark field cross-section STEM images of uniform and non-uniform regions. Footprint of an array of nanoindentations. The magnified views in (B) and (C) show individual footprints.

Acknowledgement: This work was supported by National Science Foundation grant # 1727539.

Data availability: The data that supports the findings of this study are available from the corresponding author upon reasonable request.

References

1. Tan, H.W., et al., *3D printed electronics: Processes, materials and future trends.* Progress in Materials Science, 2022. **127**: p. 100945.
2. Angel, K., et al., *Selective Electroplating of 3D Printed Parts.* Additive Manufacturing, 2018. **20**.
3. Baker, D.V., C. Bao, and W.S. Kim, *Highly Conductive 3D Printable Materials for 3D Structural Electronics.* ACS Applied Electronic Materials, 2021. **3**(6): p. 2423-2433.
4. Espera, A.H., et al., *3D-printing and advanced manufacturing for electronics.* Progress in Additive Manufacturing, 2019. **4**(3): p. 245-267.
5. Kim, C., et al., *3D Printed Electronics With High Performance, Multi-Layered Electrical Interconnect.* IEEE Access, 2017. **5**: p. 25286-25294.
6. Mohammed, M.G. and R. Kramer, *All-Printed Flexible and Stretchable Electronics.* Advanced Materials, 2017. **29**(19): p. 1604965.
7. Reiser, A., et al., *Metals by Micro-Scale Additive Manufacturing: Comparison of Microstructure and Mechanical Properties.* Advanced Functional Materials, 2020. **30**(28): p. 1910491.
8. Valentine, A.D., et al., *Hybrid 3D Printing of Soft Electronics.* Advanced Materials, 2017. **29**(40): p. 1703817.
9. Roshanghias, A., M. Krivec, and M. Baumgart, *Sintering strategies for inkjet printed metallic traces in 3D printed electronics.* Flexible and Printed Electronics, 2017. **2**(4): p. 045002.
10. Neumann, T.V. and M.D. Dickey, *Liquid Metal Direct Write and 3D Printing: A Review.* Advanced Materials Technologies, 2020. **5**(9): p. 2000070.
11. Liu, S., et al., *Laser Sintering of Liquid Metal Nanoparticles for Scalable Manufacturing of Soft and Flexible Electronics.* ACS Applied Materials & Interfaces, 2018. **10**(33): p. 28232-28241.
12. Hu, J. and M.-F. Yu, *Meniscus-Confined Three-Dimensional Electrodeposition for Direct Writing of Wire Bonds.* Science, 2010. **329**(5989): p. 313-316.
13. Zhang, X., et al., *Electrochemical gradients driven 3D printing of nano-twinned copper structures by direct current dynamic meniscus confined electrodeposition.* Applied Materials Today, 2021. **24**: p. 101138.
14. Behroozfar, A., et al., *Microscale 3D Printing of Nanotwinned Copper.* Advanced Materials, 2018. **30**(4): p. 1705107.
15. Daryadel, S., et al., *Localized Pulsed Electrodeposition Process for Three-Dimensional Printing of Nanotwinned Metallic Nanostructures.* Nano Letters, 2018. **18**(1): p. 208-214.
16. Daryadel, S., A. Behroozfar, and M. Minary-Jolandan, *Toward Control of Microstructure in Microscale Additive Manufacturing of Copper Using Localized Electrodeposition.* Advanced Engineering Materials, 2019. **21**(1): p. 1800946.

17. Morsali, R., D. Qian, and M. Minary-Jolandan, *Mechanisms of Localized Pulsed Electrodeposition (L-PED) for Microscale 3D Printing of Nanotwinned Metals.* Journal of The Electrochemical Society, 2019. **166**(8): p. D354.

18. Behroozfar, A., et al., *Additive printing of pure nanocrystalline nickel thin films using room environment electroplating.* Nanotechnology, 2020. **31**(5): p. 055301.

19. Daryadel, S., A. Behroozfar, and M. Minary-Jolandan, *A microscale additive manufacturing approach for in situ nanomechanics.* Materials Science and Engineering: A, 2019. **767**: p. 138441.

20. Bhuiyan, M.E.H., et al., *A Hybrid Process for Printing Pure and High Conductivity Nanocrystalline Copper and Nickel on Flexible Polymeric Substrates.* Scientific Reports, 2019. **9**(1): p. 19032.

21. Xu, J., et al., *Simulation and Experimental Study on Metal Microstructure of Meniscus-Confined Electrodeposition.* Advanced Engineering Materials, 2022. **24**(12): p. 2200654.

22. Burlison, S. and M. Minary-Jolandan, *Multiphysics simulation of microscale copper printing by confined electrodeposition using a nozzle array.* Journal of Applied Physics, 2022. **131**(5).

23. Bhuiyan, M.E.H., et al., *Electrical property-microstructure of copper interconnects printed by localized pulsed electrodeposition (l-PED).* Materials Letters, 2023. **330**: p. 133364.

24. Wang, C., et al., *Direct-Write Printing Copper–Nickel (Cu/Ni) Alloy with Controlled Composition from a Single Electrolyte Using Co-Electrodeposition.* ACS Applied Materials & Interfaces, 2020. **12**(16): p. 18683-18691.

25. Lee, S., et al., *Electroless Deposition-Assisted 3D Printing of Micro Circuitries for Structural Electronics.* ACS Applied Materials & Interfaces, 2019. **11**(7): p. 7123-7130.

26. Hossain Bhuiyan, M.E., et al., *Interconnect Fabrication by Electroless Plating on 3D-Printed Electroplated Patterns.* ACS Applied Materials & Interfaces, 2021. **13**(16): p. 19271-19281.

27. Mordechay Schlesinger (Editor), M.P.E., *Modern Electroplating*. 2014: John Wiley & Sons, Inc.

28. Kim, M.J., et al., *One-step electrodeposition of copper on conductive 3D printed objects.* Additive Manufacturing, 2019. **27**: p. 318-326.

29. Noam Eliaz, E.G., *Physical Electrochemistry: Fundamentals, Techniques, and Applications, 2nd Edition*. 2019: Wiley

30. Lazarus, N., et al., *Direct electroless plating of conductive thermoplastics for selective metallization of 3D printed parts.* Additive Manufacturing, 2022. **55**: p. 102793.

31. Vignesh, B., et al., *Critical assessment of high speed nanoindentation mapping technique and data deconvolution on thermal barrier coatings.* Materials & Design, 2019. **181**: p. 108084.

32. Oliver, W.C. and G.M. Pharr, *An improved technique for determining hardness and elastic modulus using load and displacement sensing indentation experiments.* Journal of Materials Research, 1992. **7**(6): p. 1564-1583.